Hydrogen Sulfide Disturbs Actin Polymerization via *S*-Sulfhydration Resulting in Stunted Root Hair Growth[1]

Jisheng Li,[a,b] Sisi Chen,[a] Xiaofeng Wang,[a] Cong Shi,[a] Huaxin Liu,[c] Jun Yang,[c] Wei Shi,[a] Junkang Guo,[c,2] and Honglei Jia[c,2,3]

[a]College of Life Sciences, Northwest A&F University, Yangling, Shaanxi 712100, China
[b]Biomass Energy Center for Arid and Semi-arid Lands, Northwest A&F University, Yangling, Shaanxi 712100, China
[c]School of Environmental Science and Engineering, Shaanxi University of Science and Technology, Xi'an, Shaanxi 710021, China

ORCID IDs: 0000-0003-3061-8998 (J.L.); 0000-0002-2450-7063 (S.C.); 0000-0002-5969-062X (H.J.)

Hydrogen sulfide (H_2S) is an important signaling molecule in plants. Our previous report suggested that H_2S signaling affects the actin cytoskeleton and root hair growth. However, the underlying mechanisms of its effects are not understood. *S*-Sulfhydration of proteins is regulated directly by H_2S, which converts the thiol groups of cysteine (Cys) residues to persulfides and alters protein function. In this work, we studied the effects of *S*-sulfhydration on actin dynamics in Arabidopsis (*Arabidopsis thaliana*). We generated transgenic plants overexpressing the H_2S biosynthesis-related genes *L-CYSTEINE DESULFHYDRASE* (*LCD*) and *D-CYSTEINE DESULFHYDRASE* in the *O-acetylserine(thiol)lyase isoform a1* (*oasa1*) mutant and Columbia-0 backgrounds. The H_2S content increased significantly in overexpressing *LCD*/*oasa1* plants. The density of filamentous actin (F-actin) bundles and the F-actin/globular actin ratio decreased in overexpressing *LCD*/*oasa1* plants. *S*-Sulfhydration also was enhanced in overexpressing *LCD*/*oasa1* plants. An analysis of actin dynamics suggested that *S*-sulfhydration inhibited actin polymerization. We also found that ACTIN2 (ACT2) was *S*-sulfhydrated at Cys-287. Cys-287 is adjacent to the D-loop, which acts as a central region for hydrophobic and electrostatic interactions and stabilizes F-actin filaments. Overaccumulation of H_2S caused the depolymerization of F-actin bundles and inhibited root hair growth. Introduction of *ACT2* carrying a Cys-287-to-Ser mutation into an *act2-1* mutant partially suppressed H_2S-dependent inhibition of root hair growth. We conclude that H_2S regulates actin dynamics and affects root hair growth.

Hydrogen sulfide (H_2S) has important physiological functions in regulating the nervous and cardiovascular systems; thus, H_2S is recognized as the third endogenous gasotransmitter, following the discovery of nitric oxide and carbon monoxide (Tan et al., 2010). In plants, Cys metabolism is related closely to H_2S generation. Cys desulfhydrases contribute to H_2S generation (Papenbrock et al., 2007). L-CYSTEINE DESULFHYDRASE (LCD) and D-CYSTEINE DESULFHYDRASE (D-CDES) degrade Cys to H_2S, pyruvate, and ammonia and are responsible for the release of H_2S into the cell (Kopriva, 2006). Both Arabidopsis (*Arabidopsis thaliana*) LCD and D-CDES-deficient mutants (*lcd* and *dcdes*, respectively) have been shown to reduce the concentration of endogenous H_2S (Hou et al., 2013). However, the activity of D-CDES is lower than that of LCD. Cys metabolism also closely relates to H_2S production. *O*-ACETYLSERINE(THIOL)LYASE (OAS-TL) catalyzes the formation of Cys by incorporating the sulfide into OAS (Sirko et al., 2004). *oastlA* and *oastlC* mutants are compromised in their ability to detoxify H_2S and, as a result, sulfide concentrations are elevated in cells (Heeg et al., 2008).

In plant systems, recent evidence indicates that H_2S acts as an important messenger that affects abiotic stress responses to high salinity, drought, heat shock, heavy metals, and oxidative stress (Chen et al., 2013; Christou et al., 2013; Li et al., 2013, 2014). Moreover, H_2S signaling has been shown to modulate important physiological processes, such as photosynthesis, immunity, cell senescence, root growth, and stomatal closure (Wang, 2012; Hou et al., 2013; Jia et al., 2015). Although many studies have described the physiological effects of H_2S in plants, its underlying mechanisms are poorly understood. Posttranslational modification of Cys residues to form persulfide groups (conversion of Cys-SH groups to Cys-SSH groups) is regulated directly by H_2S (Paul and Snyder, 2012). This process is called *S*-sulfhydration and is similar to *S*-nitrosylation. In general, *S*-nitrosylation diminishes Cys reactivity and *S*-sulfhydration enhances it; however, this is not always the case. For example, *S*-sulfhydration inhibits the activity of PROTEIN TYROSINE PHOSPHATASES1B

[1]This work was supported by the National Natural Science Foundation of China (grant nos. 31700445 and 31400246), the Shaanxi Province Natural Science Foundation of China (grant nos. 2018JM3017 and 2018JQ3020), and the Northwest A&F University Basic Research Foundation (grant no. 2452018156).

[2]Senior authors.

[3]Author for contact: jiahonglei@sust.edu.cn.

The author responsible for distribution of materials integral to the findings presented in this article in accordance with the policy described in the Instructions for Authors (www.plantphysiol.org) is: Honglei Jia (jiahonglei@sust.edu.cn).

H.L.J., J.S.L., and J.K.G. conceived and designed the experiments; J.S.L., S.S.C., X.F.W., C.S., J.Y., H.X.L., and W.S. performed the experiments; H.L.J. and J.S.L. analyzed data and wrote the article.

www.plantphysiol.org/cgi/doi/10.1104/pp.18.00838

(Krishnan et al., 2011) and *S*-nitrosylation activates CYCLIN-DEPENDENT PROTEIN KINASE5 (Qu et al., 2011). Recent evidence indicates that *S*-sulfhydration by endogenous H_2S regulates the functions of certain proteins, such as ASCORBATE PEROXIDASE1 and GLYCERALDEHYDE 3-PHOSPHATE DEHYDROGENASE (Aroca et al., 2015, 2017b).

The actin cytoskeleton is an important component of the cellular architecture and is involved in a variety of cellular activities, including establishing cell polarity, cell division, elongation, cytoplasmic streaming, vesicle transport, and organelle movement (Fowler and Quatrano, 1997; Staiger, 2000; Zhou et al., 2015). The actin cytoskeleton is a highly dynamic structure that enables rapid responses to intracellular signaling molecules and regulatory proteins (Staiger et al., 1997; Zhu et al., 2013). It has been demonstrated that dynamic actin cytoskeleton rearrangements are regulated by a pool of actin-binding proteins and phytohormones (Hussey et al., 2006; Lanza et al., 2012; Jia et al., 2013; Zhu et al., 2017). Additionally, proteomic studies have shown that cytoskeletal proteins are regulated by a variety of posttranslational modifications, including phosphorylation, *S*-glutathionylation, nitration, *S*-sulfhydration, and *S*-nitrosylation (Lam et al., 2010; Yemets et al., 2011). It was shown recently that *S*-nitrosylation of the actin cytoskeleton changes actin dynamics (Rodríguez-Serrano et al., 2014). Therefore, posttranslational modifications may be an important means of regulating actin cytoskeleton dynamics, although their functions and physiological relevance have yet to be elucidated.

Arabidopsis contains eight actin genes that are grouped into two major classes based on their roles in vegetative and reproductive organs (McDowell et al., 1996; Meagher et al., 1999). The vegetative group of actins consists of ACT2, ACT7, and ACT8 (McDowell et al., 1996; Meagher et al., 1999). Very recently, endogenous *S*-sulfhydration was demonstrated in Arabidopsis, and quantitative data indicate that persulfides are widespread in plants cells, including on ACT2 and ACT8 (Aroca et al., 2017a). Although protein *S*-sulfhydration is a direct result of H_2S signaling, reports describing the effects of H_2S signaling on actin cytoskeleton dynamics are scarce. Our published research has demonstrated that H_2S signaling affects the actin cytoskeleton in root cells. In this work, we conducted a follow-up investigation into the effects of H_2S signaling on actin *S*-sulfhydration and the resulting changes to the structure and dynamics of the actin cytoskeleton.

RESULTS

Overexpression of the *LCD* Gene in *oasa1* Mutants Significantly Increases the Endogenous H_2S Content of Arabidopsis Roots

NaHS is an H_2S donor that alters the endogenous H_2S levels in plants. Treatment with NaHS affected the growth and development of plants (Jia et al., 2015). Exogenous application of NaHS inhibited root and root hair growth in a dose-dependent manner (Supplemental Fig. S1A). After NaHS treatment, epidermal cells expanded and axial growth was inhibited in the hypocotyl (Supplemental Fig. S1B). Additionally, the size of cortex cells changed in the meristematic zone of the root (Supplemental Fig. S1, C and D).

To further decipher the function of endogenous H_2S signaling, we obtained T-DNA insertion lines for H_2S metabolism-related genes and isolated *lcd*, *dcdes*, and *oasa1* homozygous mutants. We also established endogenous H_2S overproduction lines. The *LCD* and *DCDES* genes were overexpressed in wild-type (Columbia-0 [Col-0]) or *oasa1* mutant plants under the control of the 35S promoter (Fig. 1A; Supplemental Fig. S2A). The histochemical GUS staining patterns of *LCD*::*GUS* and *DCDES*::*GUS* in transgenic seedlings showed that the *LCD* and *DCDES* genes are expressed in roots, shoots, and leaves (Supplemental Fig. S2C). The endogenous H_2S content was analyzed in mutants and transgenic lines. The H_2S content increased slightly in the overexpressing (OE) *LCD-1*, OE *LCD-3*, *oasa1*, and OE *DCDES*/*oasa1* lines and was enhanced significantly in the OE *LCD-3*/*oasa1* and OE *LCD-5*/*oasa1* lines. However, it decreased in the *lcd* and *dcdes* mutants compared with the wild-type control (Fig. 1C; Supplemental Fig. S2D). Following the application of NaHS, from 3 to 6 h, the endogenous H_2S content increased in wild-type, *oasa1*, OE *LCD-1*, OE *LCD-3*/*oasa1*, and OE *LCD-5*/*oasa1* plants (Fig. 1D). From 6 to 24 h, the endogenous H_2S level decreased in wild-type, *oasa1*, and OE *LCD-1* plants. Notably, the level of H_2S remained high in OE *LCD-3*/*oasa1* and OE *LCD-5*/*oasa1* plants (Fig. 1D).

Next, we tested the mutant and transgenic lines for sensitivity to NaHS by transferring 4-d-old seedlings to agar plates containing the same medium either with or without NaHS. The lengths of the primary root and root hairs were measured 4 d later. The root and root hair lengths of the OE *LCD-3*/*oasa1* and OE *LCD-5*/*oasa1* plants were shorter compared with those of wild-type plants (Fig. 2, A–D). The root and root hair lengths of the OE *DCDES* and OE *DCDES*/*oasa1* plants were similar to those of wild-type plants (Supplemental Fig. S3). NaHS treatment inhibited primary root elongation in the mutant and transgenic lines (Fig. 2B; Supplemental Fig. S3A). *lcd* plants grew more than wild-type plants on medium containing 100 μM NaHS. On the contrary, the root and root hairs of OE *LCD-3*/*oasa1* and OE *LCD-5*/*oasa1* plants were shorter compared with those of wild-type plants when grown on medium containing 100 μM NaHS (Fig. 2, A–D). In our previous work, we presented pharmacological evidence showing that the H_2S donors NaHS and GYY4137 cause a significant decrease in Arabidopsis root hair density (Jia et al., 2015). Consistent with our previous report, NaHS treatment decreased the root hair density in both Col-0 and the transgenic lines (Fig. 2C). Additionally, root hair initiation was delayed in *LCD-3*/

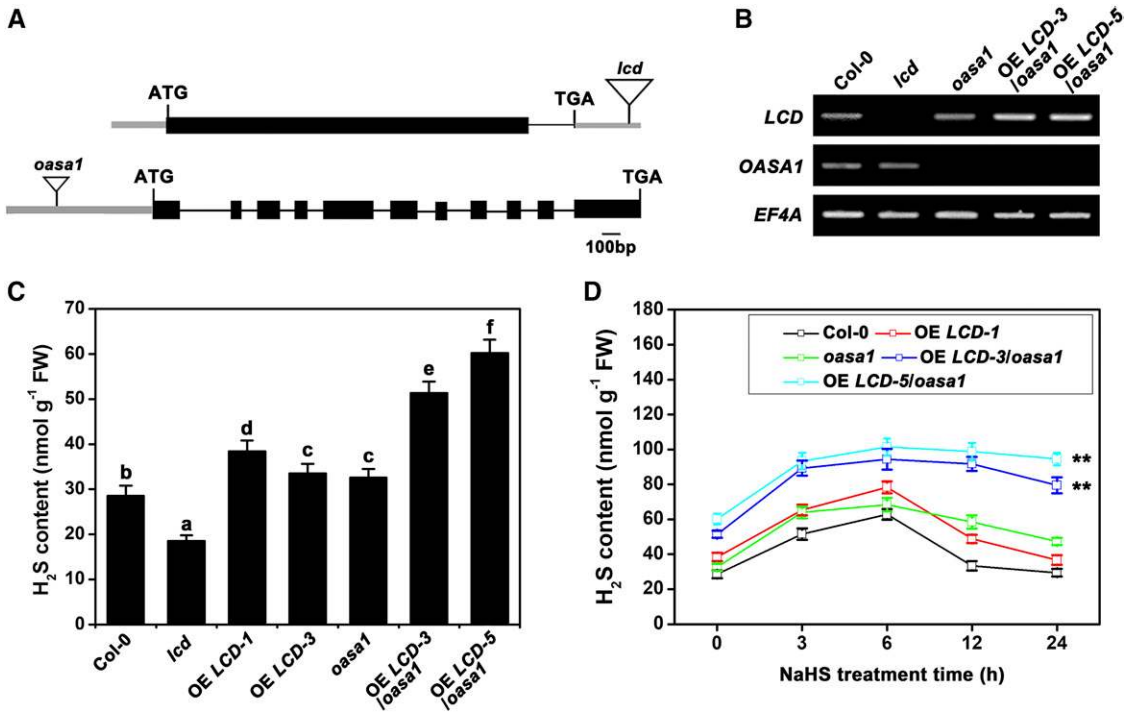

Figure 1. H_2S content assays. A, Diagrams of *LCD* and *OASA1* showing the positions of the T-DNA insertions. B, Semi-quantitative reverse transcription-polymerase chain reaction (RT-PCR) analysis with the *LCD*, *OASA1*, and *EF4A* primers using total RNA extracted from wild-type Col-0, *lcd*, *oasa1*, OE *LCD-3/oasa1*, and OE *LCD-5/oasa1* seedlings as the template. C and D, H_2S content assays. The roots of 7-d-old Arabidopsis seedlings grown in control medium (one-half-strength Murashige and Skoog agar medium with 1% Suc) were used for C. Seven-day-old Arabidopsis seedlings that were transferred to medium containing 200 μM NaHS were used for D. FW, Fresh weight. The data are means ± SE ($n = 3$). Within each set of experiments, bars with different letters are significantly different (Duncan's multiple range tests: $P < 0.05$; Student's *t* test: *, $P < 0.05$ and **, $P < 0.01$).

oasa1 and OE *LCD-5/oasa1* plants compared with wild-type plants. The NaHS-induced delay of root hair initiation also was more severe in *LCD-3/oasa1* and OE *LCD-5/oasa1* plants (Fig. 2E).

The growth of Arabidopsis decreases when the biosynthesis of Cys is inhibited (Heeg et al., 2008; Álvarez et al., 2012). On the contrary, the bolting of Arabidopsis is earlier when Cys content increases (Alvarez et al., 2010; Romero et al., 2014). Other than root morphogenesis, shoot growth decreased in OE *LCD-3/oasa1* and OE *LCD-5/oasa1* lines. As shown in Supplemental Figure S4, the shoots of the OE *LCD-3/oasa1* and OE *LCD-5/oasa1* lines were smaller compared with those of Col-0 after 6 weeks of growth. The relative weight of the OE *LCD-3/oasa1* and OE *LCD-5/oasa1* lines also decreased (Supplemental Fig. S4).

The H_2S Signal Regulates the Structure of the Actin Cytoskeleton in Arabidopsis Roots and Root Hairs

In a previous study, we showed that the H_2S signal affected the structure of the actin cytoskeleton, but we did not determine the mechanism behind this response (Jia et al., 2015). In this study, we analyzed the effect of H_2S signaling on the structure of the actin cytoskeleton by staining tissues from wild-type, *oasa1*, OE *LCD-3/oasa1*, and OE *LCD-5/oasa1* plants with fluorescein phalloidin. Seedlings were transferred to agar plates with or without NaHS for 6 h, and the actin cytoskeleton was observed in the root hairs and epidermal cells. Without NaHS treatment, the F-actin bundles appeared to be somewhat less dense in OE *LCD-3/oasa1* and OE *LCD-5/oasa1* plants than in wild-type plants in both root hair and epidermal cells (Fig. 3, A, E, G, K, O, and Q). The *oasa1* seedlings had similar amounts of F-actin bundles to the wild-type seedlings (Fig. 3, C and M). After NaHS treatment, the percentage of the field of view occupied by F-actin bundles decreased in wild-type and mutant plants (Fig. 3, I and S). However, after treatment with NaHS, there were obvious and significant differences in the cells from OE *LCD-3/oasa1* and OE *LCD-5/oasa1* plants compared with those from wild-type plants (Fig. 3, B, F, H, L, P, and R). OE *LCD-3/oasa1* and OE *LCD-5/oasa1* plants were more sensitive to NaHS than wild-type and *oasa1* plants. The percentage of F-actin bundles also decreased in leaf epidermal cells of OE *LCD-3/oasa1* and OE *LCD-5/oasa1* lines (Supplemental Fig. S5). The degree of F-actin bundling was measured by skewness (Higaki et al., 2010; Scheuring et al., 2016; Zhu et al., 2016). Application

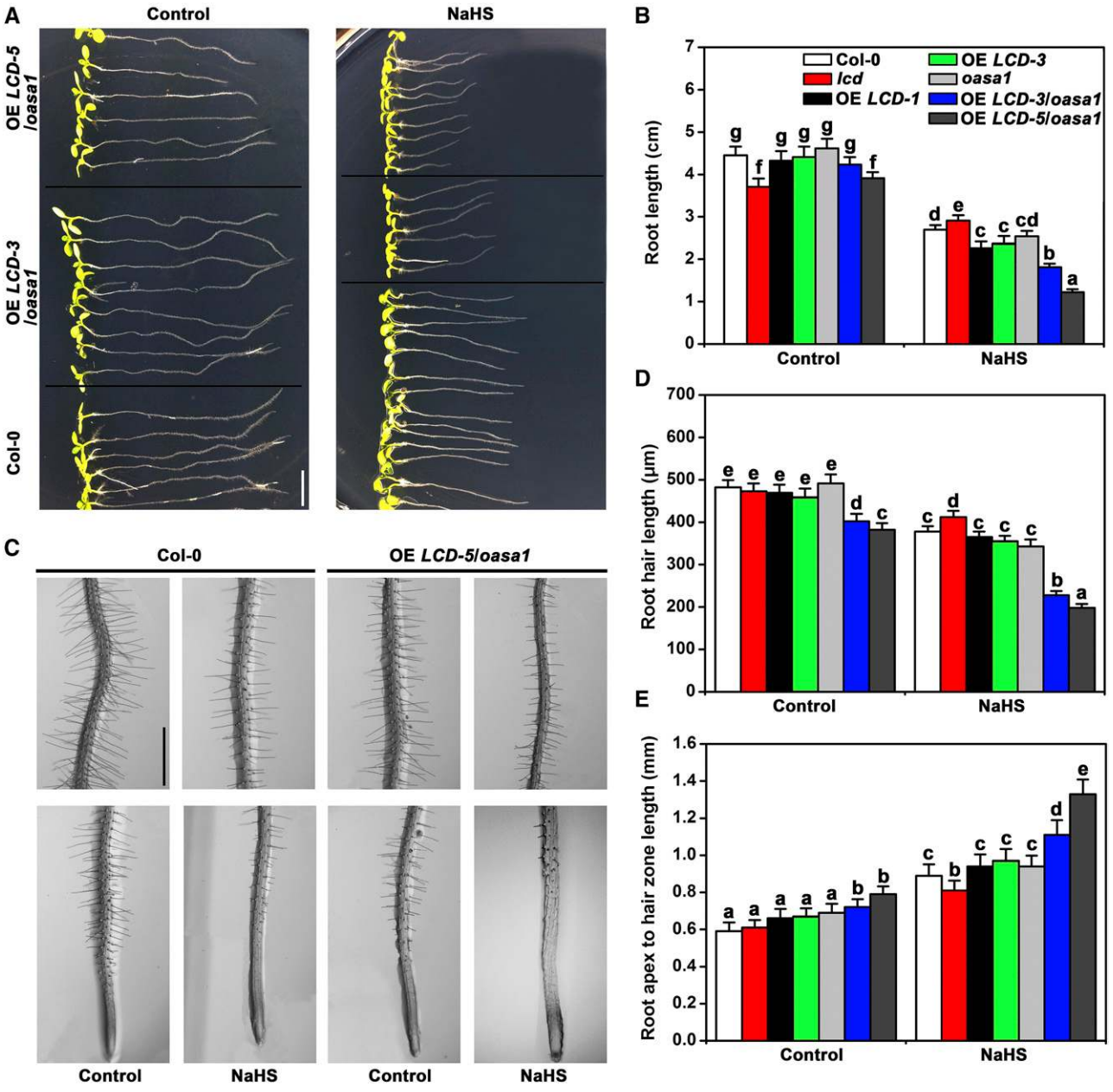

Figure 2. H_2S inhibited root and root hair growth. A, Photographs of seedlings 7 d after transfer to either control medium or medium containing 200 μM NaHS. Seedlings were transferred when they were 4 d old and had equal root lengths at that time. Bar = 1 cm. B, Quantification of the root lengths of the treated seedlings shown in A. The data are means ± SE (n = 28). C, Photographs of root hairs at the primary root tip formed after 48 h with or without 100 μM NaHS. The images shown are representative of each treatment. Bar = 1 mm. D, Quantification of root hair lengths for the seedlings shown in C. The data are means ± SE (n = 25 and at least five roots were measured). E, Length from the root apex to a root hair for the seedlings shown in C. The data are means ± SE (n = 25). Within each set of experiments, bars with different letters are significantly different at $P < 0.05$ (Duncan's multiple range tests).

of NaHS decreased the skewness of F-actin bundles in both wild-type and mutant plants (Fig. 3, J and T), implying that the degree of F-actin bundling was weakened by H_2S signal.

It is known that actin polymerization has an important influence on the structure of the actin filament network. Therefore, we analyzed the effect of the H_2S signal on the globular actin (G-actin) and F-actin contents in root extracts. As shown in Figure 4, A and B, the G-actin/F-actin ratio increased significantly in the presence of NaHS for 6 h in a dose-dependent manner. The total actin protein in extracts also was analyzed

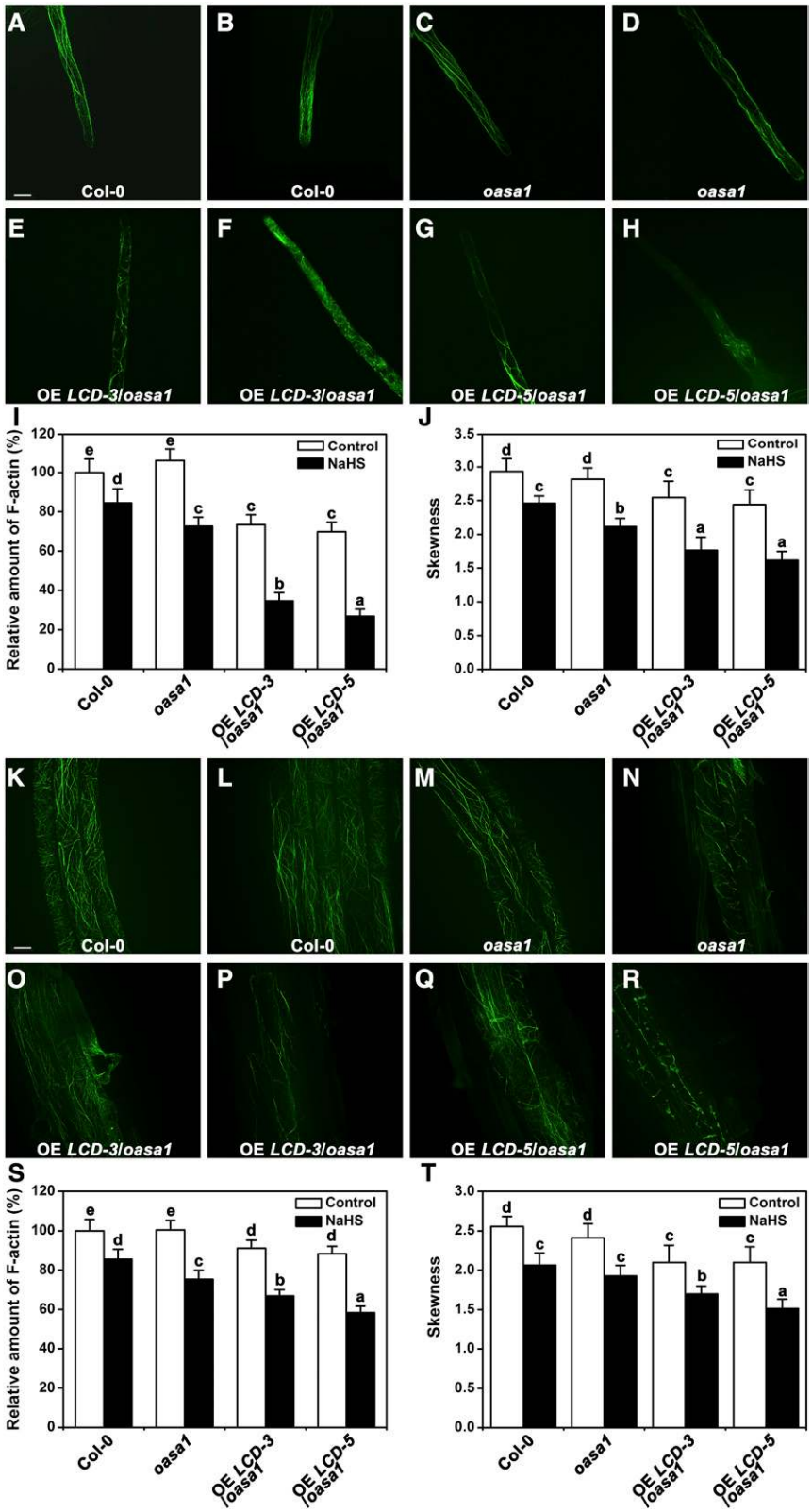

Figure 3. F-actin cytoskeletal organization assays in Col-0 (A, B, K, and L), *oasa1* (C, D, M, and N), OE *LCD-3/oasa1* (E, F, O, and P), and OE *LCD-5/oasa1* (G, H, Q, and R). A to H, Cellular phenotypes of F-actin cytoskeletal organization in root hairs. K to R, Cellular phenotypes of F-actin cytoskeletal organization in root epidermal cells. Seven-day-old Arabidopsis seedlings were transferred to medium without NaHS (A, C, E, G, K, M, O, and Q) or with 600 μM NaHS (B, D, F, H, L, N, P, and R) for 6 h. I, Quantification of the amount of F-actin in root hairs. J, Skewness analysis of F-actin in root hairs. S, Quantification of the amount of F-actin in root epidermal cells. T, Skewness analysis of F-actin in root epidermal cells. The data are means ± SE (n = 25). Within each set of experiments, bars with different letters are significantly different at $P < 0.05$ (Duncan's multiple range tests). Bars = 25 μm.

by western blotting using an anti-ACTIN antibody. No differences were detected in terms of total protein between the control and plants treated with different NaHS concentrations for 6 h, suggesting that actin was not down-regulated or proteolytically degraded by NaHS treatment (Fig. 4, C and D). The G-actin/F-actin ratio increased in OE *LCD-5/oasa1* plants in the control treatment. Treatment with 100 μM NaHS further increased the G-actin/F-actin ratio (Fig. 4, E and F). However, the total amount of actin did not change under the NaHS treatment (Fig. 4, G and H).

S-Sulfhydration Is Enhanced in Vivo in H_2S-Overproducing Transgenic Lines and Mutants

The biotin switch method (BSM) has been used to detect *S*-nitrosylation. In this work, a modified BSM was used for *S*-sulfhydration analysis (Mustafa et al., 2009). Total root protein extracts from Arabidopsis seedlings grown under control conditions were used for the BSM, and total *S*-sulfhydrated proteins were analyzed by immunoblotting with antibodies against biotin. A large array of proteins was clearly detected by the antibody in the mutants and transgenic lines. The amount of labeled proteins increased significantly in samples from OE *LCD-5/oasa1* and was enhanced slightly in *oasa1* and OE *LCD-1* samples compared with samples from Col-0 (Fig. 5A). By contrast, the labeled proteins decreased in *lcd* samples (Fig. 5A). Additionally, protein extracts that were not subjected to the modified BSM did not show any proteins labeled with biotin (Fig. 5A). Biotin-labeled proteins were isolated further and then analyzed by immunoblotting with antibodies against actin. The results indicate that actin protein underwent *S*-sulfhydration. The *S*-sulfhydration of actin increased in OE *LCD-5/oasa1*, *oasa1*, and OE *LCD-1*, but decreased in *lcd*, compared with the wild type (Fig. 5, C and D). *S*-Sulfhydration was abolished by the application of DTT (Fig. 5C). The total amount of actin did not change in the mutant and transgenic lines (Fig. 5C).

In Vitro Detection of *S*-Sulfhydration of ACT2, ACT7, and ACT8 and the Location of *S*-Sulfhydration Sites in ACT2

ACT2, ACT7, and ACT8 regulate vegetative growth in Arabidopsis. To determine whether ACT2, ACT7, or ACT8 was *S*-sulfhydrated in the presence of NaHS, recombinant ACT2, ACT7, and ACT8 were purified. These purified proteins were labeled with biotin and detected subsequently by an antibiotin immunoblot analysis. The results indicated that NaHS induced *S*-sulfhydration of ACT2, ACT7, and ACT8 in a dose-dependent manner and that *S*-sulfhydration was abolished by the application of DTT (Fig. 6A). Four Cys residues in ACT2, ACT7, and ACT8 are putative target sites of *S*-sulfhydration. We carried out liquid chromatography-tandem mass spectrometry analysis of the recombinant ACT2 protein. The mass of Cys-287 increased, which suggested that this residue had gained a sulfhydryl modification (Fig. 5; Supplemental Fig. S6). To determine whether the Cys-287 residue is required for NaHS-mediated *S*-sulfhydration, we separately mutated each Cys (C) in ACT2 to a Ser (S) and tested the effect of NaHS on the modified proteins. Of the four mutations, only the Cys-287Ser (C287S) mutation eliminated *S*-sulfhydration by NaHS (Fig. 6B). These data suggest that ACT2 is *S*-sulfhydrated at Cys-287 in the presence of H_2S donors.

S-Sulfhydration Regulates Actin Dynamics

Actins from animals and plants have high sequence similarity. Cys-287 is conserved in actin from rabbit muscle (Supplemental Fig. S7A). Additionally, the *S*-sulfhydration levels in actin from rabbit muscle increased when treated with NaHS and were reversed by DTT (Supplemental Fig. S7B). This rabbit muscle actin was extracted and used to test directly whether the H_2S signal affected actin dynamics. The formation of F-actin bundles was visualized by fluorescence microscopy in vitro. Long and thick F-actin bundles were observed in the control condition. In contrast, fewer and shorter F-actin bundles were observed with increasing concentrations of NaHS (Fig. 7, A and B). The effect of NaHS on F-actin bundles was abolished by DTT (Fig. 7, A and B). Actin nucleation is the limiting step of actin polymerization. To further confirm the role of *S*-sulfhydration in actin dynamics, the effect of NaHS on the polymerization of actin monomers was investigated. As shown in Figure 7C, when pyrene fluorescence was used to monitor the actin polymerization kinetics, the initial lag that corresponds to the nucleation step decreased with increasing concentrations of NaHS, and this occurred in a dose-dependent manner. We examined the behavior of individual actin filaments at steady state with time-lapse total internal reflection fluorescence (TIRF) microscopy. Protein was incubated with or without NaHS for 20 min, and the growth of actin filaments was captured over a 10-min period (Fig. 7, D and E; Supplemental Movies S1–S3). Under the control condition, actin filaments formed rapidly at an average rate of 3.5 ± 0.43 subunits s^{-1} (Fig. 7, E and F). The decrease in filament lengths in the NaHS treatments was dose dependent. In the presence of 400 or 600 μM NaHS, the filaments were significantly shorter and their elongation was reduced by approximately 2.7 or 1.6 subunits s^{-1}, respectively (Fig. 7, E and F). These results suggest that H_2S-induced actin *S*-sulfhydration may inhibit actin polymerization.

The C287S Mutation in ACT2 Partially Suppresses the Effect of NaHS on the Growth of Root Hairs

ACT2 Cys-287 is modified by *S*-sulfhydration, and H_2S negatively regulates the growth of actin filaments by *S*-sulfhydration in vitro. Therefore, we hypothesized that H_2S-induced ACT2 *S*-sulfhydration may affect root hair growth by regulating the structure of the actin cytoskeleton in vivo. To test this hypothesis,

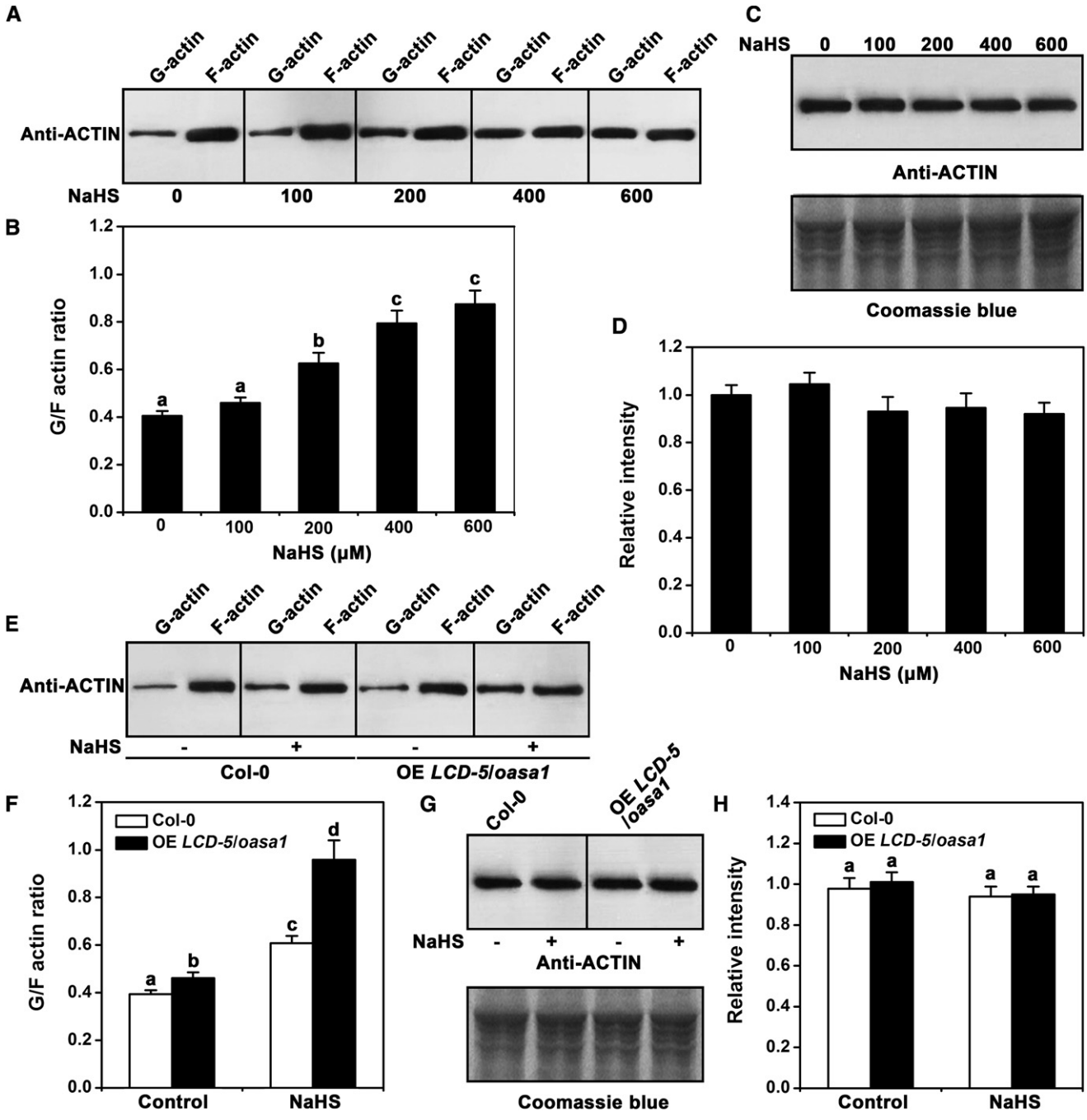

Figure 4. In vivo western-blot actin polymerization assays. Seven-day-old Arabidopsis seedlings were transferred to medium with or without NaHS for 6 h. An equal volume of root protein was used for each fraction. A to D, NaHS treatments at 100 to 600 μM. E to H, NaHS treatments at 100 μM. A and E, Effects of NaHS on the F-actin/G-actin ratio in Col-0 (A) and OE *LCD-5/oasa1* (E). B, Quantification of the F-actin/G-actin ratio for the samples shown in A. F, Quantification of the F-actin/G-actin ratio for the samples shown in E. C and G, Effects of NaHS on the total actin in Col-0 (C) and OE *LCD-5/oasa1* (G). D, Quantification of the total actin for the samples shown in C. H, Quantification of the total actin for the samples shown in G. The data are means ± SE ($n = 3$). Within each set of experiments, bars with different letters are significantly different at $P < 0.05$ (Duncan's multiple range tests).

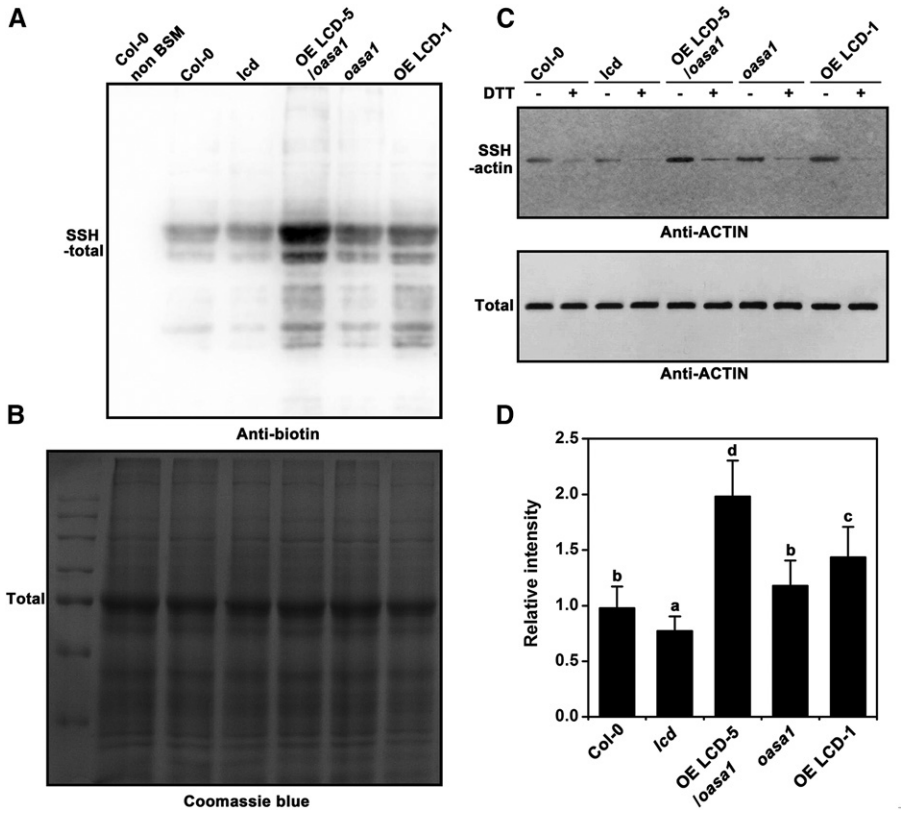

Figure 5. In vivo *S*-sulfhydrated actin protein assays. A, Immunoblot analysis of the total *S*-sulfhydrated protein in seedling roots. Protein was extracted from cells in the root tissue. *S*-Sulfhydrated proteins were labeled with biotin and analyzed using a biotin antibody. B, Total protein loading is indicated by Coomassie Blue staining. C, Immunoblot analysis of *S*-sulfhydrated actin and immunoblot analysis of the total actin. Biotinylated proteins obtained from the root extracts were subjected to a modified BSM assay, were purified using streptavidin-agarose beads, and were analyzed using an actin antibody (top). Total protein extracts from root tissue also were analyzed using actin antibody (bottom). D, Quantification of the *S*-sulfhydration shown in C. The data are means ± SE ($n = 3$). Within each set of experiments, bars with different letters are significantly different at $P < 0.05$ (Duncan's multiple range tests).

we isolated *act2-1/ACT2*^{C287S} mutant plants in which *ACT2* expression was driven by the native promoter. The phenotypes of *act2-1* were fully rescued in *act2-1/ACT2*^{WT} and partly rescued in *act2-1/ACT2*^{C287S} (Fig. 8A). In *act2-1/ACT2*^{C287S} mutants, NaHS was substantially less effective at inhibiting root hair growth than in *act2-1/ACT2*^{WT} (Fig. 8B). To further investigate the responses of the mutant and transgenic lines to the H_2S signal, time-lapse images of root hair growth were captured over a 20-min period (Supplemental Movies S4–S11). Without NaHS treatment, OE *LCD-5/oasa1* plants had significantly lower rates of root elongation (Fig. 8C). After NaHS treatment, the rate of root elongation decreased significantly in *act2-1/ACT2*^{WT}, OE *LCD-5/oasa1*, and OE *LCD-1*. However, the effect of NaHS on the rate of root elongation was noticeably less in *act2-1/ACT2*^{C287S} (Fig. 8C). Additionally, the effect of NaHS on the amount of F-actin bundles also was weakened in root hairs from *act2-1/ACT2*^{C287S} mutants (Fig. 8, D and E).

DISCUSSION

The H_2S signal regulates a number of processes related to growth and abiotic stress responses in plants. The application of exogenous H_2S donors that enhance H_2S signaling is a typical method for exploring the function of the H_2S signal. Because of H_2S metabolism and the stability of H_2S donors, the H_2S content is labile during H_2S donor treatment (Fig. 1F). Isolating H_2S-overproducing lines is a reliable way to study the function of the H_2S signal in plants. LCD and D-CDES are the key enzymes that contribute to H_2S generation. However, the content of H_2S only increased slightly in the *LCD*-overexpressing transgenic lines and did not change in the *DCDES*-overexpressing line. H_2S metabolism is a complex process that is closely related to Cys metabolism (Heeg et al., 2008). OAS-TL incorporates H_2S into OAS (Sirko et al., 2004). The activity of OAS-TL decreased by approximately 50% in the *oasa1* mutant (Heeg et al., 2008). Therefore, we overexpressed the *LCD* or *DCDES* gene in *oasa1*. Interestingly, the H_2S content was increased significantly in the OE *LCD/oasa1* lines and the high H_2S level appeared to persist (Fig. 1). These studies thus offer a new strategy for exploring the physiological function of H_2S in plants.

The actin cytoskeleton is a major factor in the cellular response to plant signaling molecules. Brassinosteroids alter actin filament organization, resulting in an altered gravitropism phenotype in Arabidopsis roots (Lanza et al., 2012). Auxin modulates its own transport simply by fine-tuning the configuration of actin microfilaments (Nick et al., 2009). Nitric oxide can induce actin depolymerization in sycamore (*Acer pseudoplatanus*) tree cells, and this process also has been associated with the induction of programmed cell death (Malerba et al., 2008). In our previous work, we demonstrated

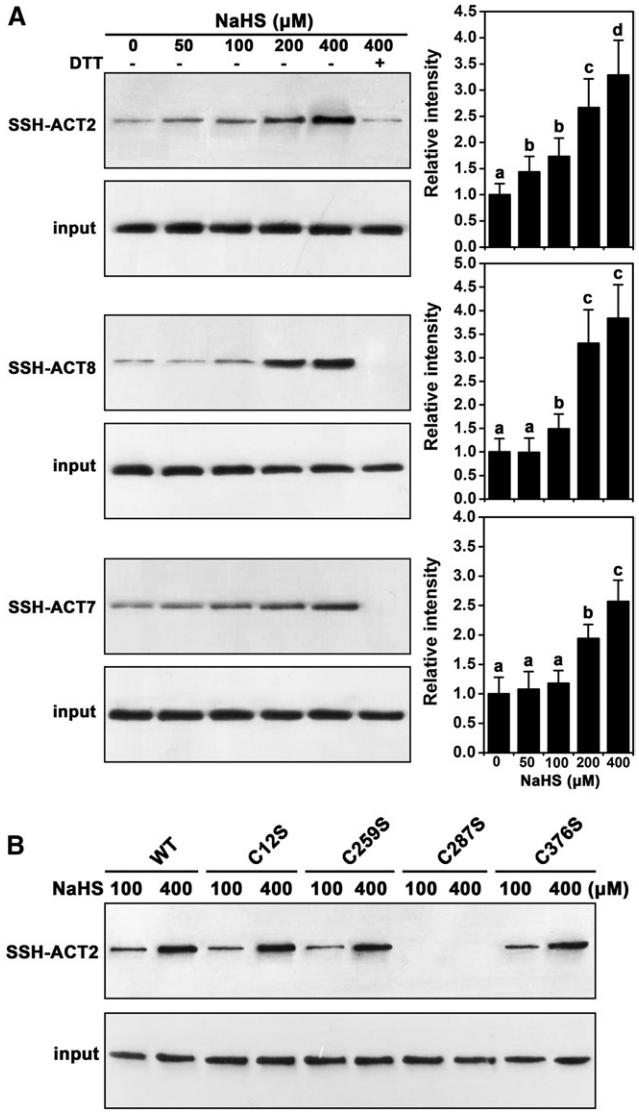

Figure 6. Immunoblot analysis of recombinant actin proteins from vegetative tissues. A, NaHS-induced *S*-sulfhydration of ACT2, ACT8, and ACT7 was detected using a biotin-switch assay. *S*-Sulfhydrated proteins were labeled with biotin and analyzed using a biotin antibody. Graphs at right show the quantification of *S*-sulfhydration levels in ACT2, ACT8, and ACT7. Proteins were incubated with the indicated concentrations of NaHS or NaHS plus DTT (10 mM) for 20 min. The data are means ± SE ($n = 3$). B, Effects of C-to-S site-directed mutagenesis on *S*-sulfhydration of the four Cys residues in ACT2 following NaHS treatment. Within each set of experiments, bars with different letters are significantly different at $P < 0.05$ (Duncan's multiple range tests). WT, Wild type.

that 200 μM of an H_2S donor affects F-actin, leading to a reduction in the actin cytoskeleton (Jia et al., 2015). Although F-actin can be visualized by confocal microscopy, quantification by fluorescent labeling is subject to large error. Compared with the fluorescent label, western-blot analysis is a more accurate method for the analysis of F-actin content (Rodríguez-Serrano et al., 2014). In this work, we further analyzed the effect of NaHS on G-actin and F-actin contents under 100 to 600 μM NaHS. Consistent with our previous report, 200 μM NaHS increased the G-actin/F-actin ratio. However, 600 μM NaHS significantly increased the G-actin/F-actin ratio (Fig. 4A). In this study, a reduction in the actin cytoskeleton also was observed in the H_2S-overproducing lines OE *LCD-3/oasa1* and OE *LCD-5/oasa1* (Fig. 2; Supplemental Fig. S5). We also found that the amount of F-actin bundles increased significantly in the wild type under naphthylacetic acid (NAA) treatment (Supplemental Fig. S8A; Scheuring et al., 2016). However, the effect of NAA was weakened in the OE *LCD-5/oasa1* line and by NaHS treatment (Supplemental Fig. S8, A, C, and D). The degree of F-actin bundling was increased by NAA in both Col-0 and OE *LCD-5/oasa1* (Supplemental Fig. S8, C and E). NaHS treatment did not alter the effect of NAA on the degree of F-actin bundling (Supplemental Fig. S8, C and E). In the presence of 500 nM NAA, the growth rate of filaments increased, and this effect was reduced by NaHS (Supplemental Fig. S8, F and G). In addition, root hair growth was enhanced significantly by NAA. However, NAA-induced root hair growth was reduced by NaHS (Supplemental Fig. S9). In previous work, the effect of H_2S signaling on polar auxin transport has been reported (Jia et al., 2015), suggesting that H_2S plays an important role in modulating auxin transport by regulating the actin cytoskeleton. In this work, we present data suggesting the existence of a tightly regulated and intertwined signaling network involving H_2S, auxin, and actin that controls root system development. In the cross talk between H_2S and auxin, *S*-sulfhydration of the actin cytoskeleton may be an important factor. Taken together, these results suggested that there is a cross talk between plant signaling molecules and actin. However, the role and hierarchical relationship of plant signaling molecules and the actin cytoskeleton under physiological conditions have not being established.

More recently, it was reported that the synthetic auxin 2,4-dichlorophenoxyacetic acid affects actin polymerization through modification of the carbonylation status of actin in Arabidopsis (Rodríguez-Serrano et al., 2014). In animal cells, *S*-nitrosylation disrupts the normal growth of F-actin, resulting in the depolymerization of the actin cytoskeleton (Dalle-Donne et al., 2001). *S*-Nitrosylated G-actin polymerizes less efficiently than unmodified G-actin and, thus, forms less F-actin. Compared with unmodified actin, *S*-nitrosylated actin forms shorter F-actin bundles and reduces the distribution of the actin cytoskeleton (Dalle-Donne et al., 2000). *S*-Sulfhydration is a physiological modification of many proteins and is regulated directly by H_2S signaling. Numerous proteins have been reported to be *S*-sulfhydrated in animal cells, including actin, tubulin, and glyceraldehyde-3-phosphate dehydrogenase. In plants, persulfidation proteome data identified several actin proteins. In this study, the *S*-sulfhydration level of total actin increased significantly in the H_2S-overproducing line OE *LCD-5/oasa1* and *S*-sulfhydration

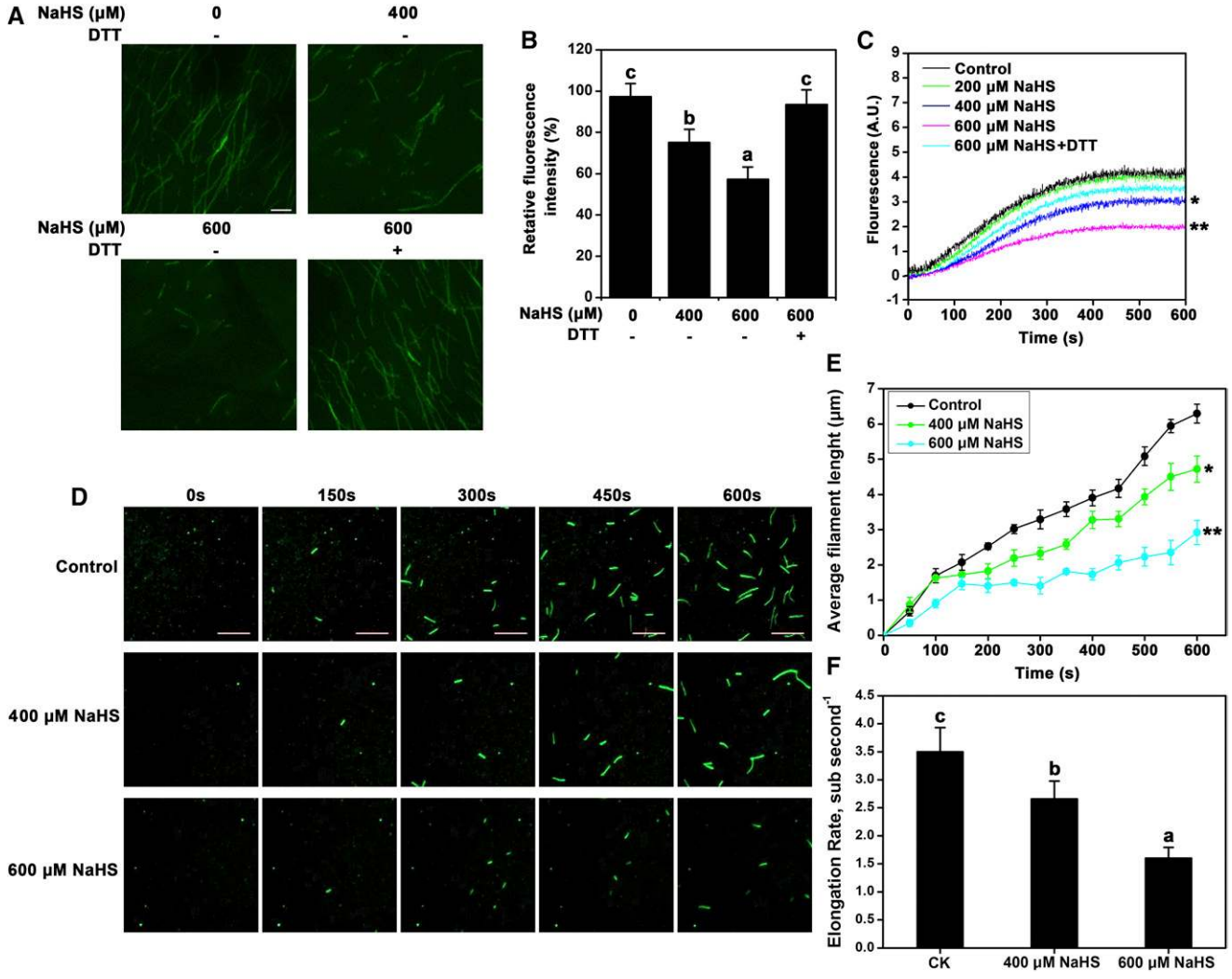

Figure 7. In vitro actin dynamics assays. A, Micrographs of F-actin bundles stained with Alexa 488-phalloidin. Prepolymerized actin (3 μM) was incubated with or without the indicated concentrations of NaHS or NaHS plus DTT (10 mM) at room temperature for 20 min. Bar = 10 μm. B, Quantification of the amount of F-actin in the samples shown in A. The data are means ± SE (n = 5). C, H_2S decreased actin nucleation. Two micromolar actin (5% pyrene labeled) was incubated for 5 min with varying concentrations of NaHS before polymerization. Pyrene fluorescence was plotted over time after the addition of polymerization buffer, A.U. represents the unit of relative light energy. D, Elongation of actin filaments visualized by TIRF. Actin monomers (1 μM, 40% rhodamine labeled) were incubated with various concentrations of NaHS and polymerized in fluorescence buffer. Image acquisition began as soon as possible and continued over a 600-s period, and the acquisition interval was 15 s (Supplemental Movies S1–S3). Bars = 10 μm. E, Measurement of changes in filament length over time. The data are means ± SE (n = 200). F, Filament elongation rates in the absence or presence of NaHS. Elongation rates were determined by measuring the filament length during actin filament elongation. Within each set of experiments, bars with different letters are significantly different (Duncan's multiple range tests: $P < 0.05$; Student's t test: *, $P < 0.05$ and **, $P < 0.01$).

modifications were detected in vivo and in vitro (Figs. 5 and 6). *S*-Sulfhydration decreased the distribution of the actin cytoskeleton in Arabidopsis cells, directly weakened actin polymerization, and inhibited the growth of F-actin bundles in vitro, and these effects were reversed by DTT (Fig. 7; Supplemental Movies S1–S3). Consequently, the altered actin cytoskeleton affected the growth of the Arabidopsis lines. *S*-Sulfhydration also alters actin cytoskeletal rearrangement in animal cells (Mustafa et al., 2009). Our previous and current work suggest that signaling molecules that influence posttranslational modification may be involved in an important molecular mechanism that regulates the actin cytoskeleton in both animals and plants.

Root hair growth was impaired in OE *LCD-5/oasa1* plants. There was no specificity for H_2S-induced actin *S*-sulfhydration. *S*-Sulfhydration modifications were detected in ACT2, ACT8, and ACT7. In plants, the amino acid sequences of the actin family proteins have high

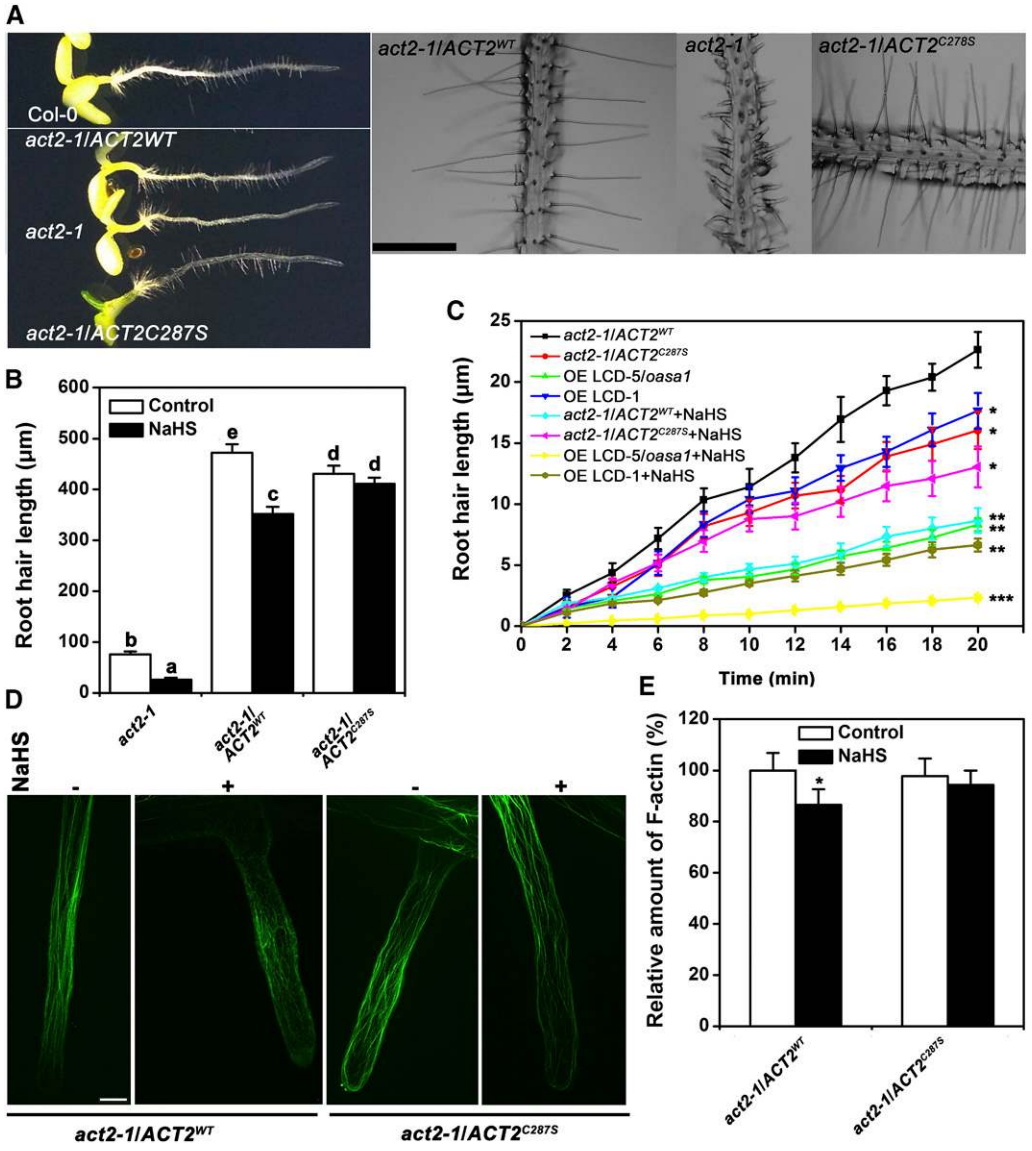

Figure 8. Cys-287 of ACT2 responds to the H_2S signal in vivo. A, Morphological phenotypes of root hair and root growth. Bar = 500 μm. B, Effects of NaHS on the root hair length at the primary root tip. Root hairs were grown in 50 μM NaHS for 48 h. The data are means ± SE (n = 25, at least five roots were measured). C, Effects of NaHS on root hair elongation over time. Five-day-old Arabidopsis seedlings were transferred to medium with or without 500 μM NaHS for 3 h, and root hair growth was measured within 20 min. Time-lapse images of root hair growth are provided in Supplemental Movies S4 to S11. The data are means ± SE (n = 5). D, Effects of NaHS on F-actin cytoskeletal organization in the root hairs of *act2-1/ACT2*^{WT} and *act2-1/ACT2*^{C278S}. Seven-day-old Arabidopsis seedlings were transferred to medium with or without 500 μM NaHS for 6 h, and the F-actin bundles in the roots were imaged. Bar = 25 μm. E, Quantification of the amount of F-actin in the root hairs shown in D. The data are means ± SE (n = 25). Within each set of experiments, bars with different letters are significantly different (Duncan's multiple range tests: $P < 0.05$; Student's t test: *, $P < 0.05$; **, $P < 0.01$; and ***, $P < 0.001$).

similarity. This may explain why *S*-sulfhydration modifications were detected in several of the actin family members. ACT2 and ACT8 are involved in root hair tip growth, and ACT2 plays a central role in this process. *act2-1* displays impaired root hair development and the lower half of the root hair (Fig. 8A). We provided evidence that the Cys-287 residue is a potential *S*-sulfhydration site in ACT2. The D-loop acts as a central region for hydrophobic and electrostatic interactions that stabilize the F-actin filament. The Asp-288 and Asp-290 residues may stabilize F-actin and the D-loop (von der Ecken et al., 2015). The Cys-287 residue is close to the Asp-288 and Asp-290 residues. By introducing *ACT2*^{WT} and *ACT2*^{C287S} under the control of the native *ACT2* promoter into the *act2-1* mutant, H_2S-induced root hair inhibition was partly restored

in *act2-1/ACT2*^{C287S} plants, suggesting that the Cys-287 residue may be a target of *S*-sulfhydration in actin proteins.

In conclusion, this work demonstrates stable H_2S overproduction in living plants and provides a genetic system for exploring the physiological functions of H_2S signaling in plants. Using this system, we showed that H_2S triggers changes in the actin cytoskeleton through the *S*-sulfhydration of actin.

MATERIALS AND METHODS

Plant Material and Chemical Treatments

This study was carried out on Arabidopsis (*Arabidopsis thaliana*), including Col-0 wild type and *lcd* (SALK_082099), *des1-1* (SALK_103855), *lcddes1-1* (*lcd* and *des1* cross), and *oasa1* (SALK_074242c) mutants (Jia et al., 2016). For the overexpressing lines, OE *LCD* and OE *DCDES*, the *LCD* and *DCDES* fragments were amplified from total cDNA and cloned into the pCAMBIA1300-35S vector with the restriction sites *Xba*I and *Kpn*I. For construction of the histochemical staining lines, the promoters of *LCD* and *DCDES* were amplified from genomic DNA and were each cloned into pBI121-GUS with the restriction sites *Xba*I and *Bam*HI. The resulting plasmids were sequenced and transformed into the Col-0 or *oasa1* mutant plants using the floral dip method. Ten independent transgenic lines were examined. Details of the site-directed ACT2 mutant constructs are provided in Supplemental Materials and Methods S1. All primers used in this study are listed in Supplemental Table S1.

Seeds were surface sterilized with 70% (v/v) ethanol for 30 s and 10% (v/v) sodium hypochlorite for 8 min and then washed five times with sterilized water before sowing on solid one-half-strength Murashige and Skoog medium (pH 5.8) containing 1% (w/v) Suc and 0.8% (w/v) agar. After that, the seeds were vernalized for 2 d at 4°C. Then, the seedlings were transferred to a growth chamber, with a temperature set to 22°C and a 14/10-h light/dark photoperiod under a photon flux of 120 µmol m^{-2} s^{-1}.

RNA Isolation and RT-PCR Analysis

Arabidopsis seedlings were harvested to extract total RNA for RT-PCR. Total mRNA was extracted using an RNAprep pure plant kit (Tiangen) and was treated with RNase-free DNase reagent (RNase-free DNase kit; Tiangen). The total mRNA was reverse transcribed into first-strand cDNA using PrimeScript Reverse Transcriptase (Takara) and oligo$(dT)_{15}$ primer (Takara) following the manufacturer's instructions. The housekeeping gene *EF4A* was used as an internal control using the primers 5′-TTGGCGGCACCCTTAGCTGGATCA-3′and 5′-ATGCCCCAGGACATCGTGATTTCAT-3′. The PCR products were electrophoresed in 1% agarose stained with ethidium bromide.

Measurement of the H_2S Content

The endogenous H_2S content was measured according to a previously described method (Chen et al., 2016). The seedlings were ground and extracted in 10 mL of phosphate-buffered saline (pH 6.8, 50 mM) containing 0.1 mM EDTA and 0.2 mM ascorbic acid. The homogenate was mixed in a test tube containing 100 mM phosphate-buffered saline (pH 7.4), 10 mM L-Cys, and 2 mM phosphopyridoxal at room temperature, and the released H_2S was absorbed in a zinc acetate trap. The trap consisted of a small glass tube containing 3 mL of 0.5% (w/v) zinc acetate that was fixed to the bottom of the reaction bottle. After a 30-min reaction, 0.3 mL of 20 mM dimethyl-*p*-phenylenediamine was dissolved in 7.2 mM HCl and added to the trap. This was followed by injection of 0.3 mL of 30 mM ferric ammonium sulfate in 1.2 mL of HCl. After incubation for 15 min at room temperature, the amount of H_2S in the zinc acetate trap was determined colorimetrically at 667 nm. A calibration curve was made by NaHS according to the above method, and H_2S content in seedlings was expressed as nmol g^{-1} fresh weight.

Root and Hair Morphology Measurements

The growth rate of root hairs was determined by time-lapse analysis (Szumlanski and Nielsen, 2009). Root hair length was observed using a Leica S8AP0 stereomicroscope. The time interval between each acquired image was 1 min over a total period of 20 min. Five root hairs per plant and three plants per genotype or treatment were scored. ImageJ was used to measure growth and to generate a video from the images.

Observation and Analysis of the Actin Cytoskeleton

The actin cytoskeleton in the root and root hairs of different transgenic lines was visualized according to a previously described method (Gibbon et al., 1999; Jia et al., 2013) with slight modifications. First, the plants were fixed with 1% polyoxymethylene and 0.025% glutaraldehyde (in 50 mM PIPES, pH 6.8) for 20 min, 2% polyoxymethylene and 0.05% glutaraldehyde for 20 min, and 4% polyoxymethylene and 0.1% glutaraldehyde for 20 min. The fixed tissues were gently washed three times with 50 mM PIPES (pH 6.8) and then subjected to actin staining with 200 nM Alexa 488-phalloidin (Molecular Probes, Invitrogen) in a buffer containing 50 mM Tris-HCl, 200 mM NaCl, and 0.05% Nonidet P-40 at pH 7.5. The F-actin was visualized subsequently using a confocal laser-scanning microscope (component Revolution-WD, microscope Leica SM IRBE Multisyne FE 1250) equipped with a 100× objective.

We used Z-stack scanning to image the dynamic variation of F-actin bundles. Samples were excited at 488 nm, and emission was recorded between 500 and 550 nm. Image capture was performed with the same confocal settings for samples in the same experiments to generate comparable images among different treatments or genetic backgrounds. Images were exported and processed using ImageJ. The amount of F-actin was analyzed by measuring the pixel intensity (intensity mm^{-2}) of individual tissues, and the images were subsequently processed and analyzed with ImageJ software by subtracting 50% of the background. F-actin bundles were measured using the skewness program component of ImageJ (Higaki et al., 2010; Scheuring et al., 2016; Zhu et al., 2016).

Western-Blot Analysis

Western-blot analysis of F-actin versus free G-actin was performed according to Rasmussen et al. (2010). Arabidopsis roots were homogenized in buffer containing 0.1 M PIPES (pH 6.9), 30% (v/v) glycerol, 5% (w/v) DMSO, 1 mM $MgSO_4$, 1 mM EGTA, 1% (v/v) Triton X-100, 1 mM ATP, and a protease inhibitor cocktail. Homogenates were centrifuged at 20,000*g* for 1 h at 4°C to separate F-actin from G-actin. F-actin from the pellet was depolymerized with cytochalasin and solubilized in an equal volume of supernatant containing 0.1 M PIPES (pH 6.9), 1 mM $MgSO_4$, 10 mM $CaCl_2$, and 5 µM cytochalasin D. After incubation for 1 h, equal volumes of both fractions were analyzed by western blot using an antibody against ACTIN (Sigma-Aldrich).

Immunochemical Detection of *S*-Sulfhydrated Actin

S-Sulfhydrated proteins were detected using a modified BSM (Mustafa et al., 2009). Arabidopsis roots were homogenized in MAE buffer (25 mM HEPES, 1 mM EDTA, 0.1 mM neocuproine, and 0.2% Triton X-100, pH 7.7) containing a complete protease inhibitor cocktail (Roche). The extract was centrifuged at 4°C for 30 min. Blocking buffer (HEN buffer supplemented with 2.5% [w/v] SDS and 20 mM methyl methanethiosulfonate (MMTS)) was added to the root extract, and the solution was incubated at 50°C for 20 min to block free sulfhydryl groups. The proteins were resuspended in HEN buffer supplemented with 1% (w/v) SDS. *S*-Sulfhydrated proteins were labeled using 4 mM biotin-HPDP (Pierce) for 3 h at 25°C in the dark. The biotinylated proteins were purified by immunoprecipitation overnight at 4°C with 15 µL of IPA (UltralLink Immobilized Protein A/G; Pierce) per mg of protein and preincubated with 2 µL of anti-biotin antibody (Sigma-Aldrich). Beads were washed three times with phosphate-buffered saline, and bound proteins were eluted with 10 mM DTT in an SDS-PAGE solubilization buffer and transferred to a polyvinylidene fluoride membrane. Actin was detected with an antibody against actin (Sigma-Aldrich).

The purified recombinant ACT2, ACT7, and ACT8 proteins were treated with 50 to 400 mM NaHS to increase the concentration of *S*-sulfhydrated protein or with 1 mM DTT to reduce all of the disulfide bonds; both treatments were carried out at 4°C for 30 min. NaHS was removed using Micro BioSpinP6 columns

(Bio-Rad). The proteins were blocked with MMTS, and the *S*-sulfhydrated Cys residues were labeled by biotin in the presence of HDPD-biotin. The S-sulfhydrated proteins were detected by immunoblot using an anti-biotin antibody (Sigma-Aldrich).

Nucleation Assay

Actin nucleation was performed essentially as described by Schafer et al. (1996). Monomeric actin (2 mM, 5% pyrene labeled) was incubated with NaHS or NaHS with DTT for 5 min in buffer G (5 mM Tris-HCl, 0.2 mM ATP, 0.1 mM $CaCl_2$, 0.5 mM DTT, and 0.1% NaN_3, pH 8). The fluorescence of pyrene-actin was monitored with a FluoroMax-4 spectrofluorometer (HORIBA Jobin Yvon) after the addition of a one-tenth volume of 10× KMEI (50 mM KCl, 1 mM $MgCl_2$, 1 mM EGTA, and 10 mM imidazole-HCl, pH 7).

Visualization of F-Actin with Fluorescence Microscopy

To visualize F-actin using fluorescence microscopy, the samples were labeled with Alexa 488-phalloidin (Molecular Probes, Invitrogen) as described previously (Jia et al., 2013). F-actin was observed using a Leica DFC420C fluorescence microscope equipped with a five-megapixel CCD camera and the Leica Application Suite software.

TIRF Microscopy

The method used for microscopy was described by Michelot et al. (2005). A spinning-disk confocal laser-scanning microscope (component Revolution-WD, microscope Leica SM IRBE Multisyne FE 1250) was used for the observation of actin filament elongation. Images were acquired at 15-s intervals during the actin polymerization time course. Glass flow cells (Amann and Pollard, 2001) were coated with 10 nM NEM-myosin for 1 min and washed with 1% BSA in fluorescence buffer as described by Michelot et al. (2005). Actin monomers (1 μM, 40% rhodamine labeled) were polymerized in fluorescence buffer (50 mM KCl, 1 mM $MgCl_2$, 10 mM imidazole, 1 mM EGTA, 100 μM $CaCl_2$, 200 μM ATP, 3 mM NaN_3, 3 mg mL^{-1} Glc, 100 μg mL^{-1} Glc oxidase, 20 μg mL^{-1} catalase, and 10 mM DTT, pH 7) in the flow cell. Images were acquired as soon as possible, and acquisition lasted for 600 s. ImageJ software (https://imagej.nih.gov/ij/) was used to determine elongation rates by measuring the filament lengths during actin filament elongation. Linear fits were made to the plots of length versus time to obtain the slope, which represented the filament elongation rate. Rates were converted from μm s^{-1} to subunits s^{-1} using an estimate of 333 actin monomers per micrometer.

Statistical Analysis

Each experiment was repeated at least three times with three replications per experiment. Values were expressed as means ± SE. For all experiments, the overall data were statistically analyzed in SPSS version 17.0 (SPSS). The statistical analysis of two groups was performed using Student's *t* test. In all cases, the confidence coefficients were set at *, $P < 0.05$; **, $P < 0.01$; and ***, $P < 0.001$. The statistical analysis of multiple groups was performed using Duncan's multiple range tests. In all cases, the confidence coefficient was set at 0.05.

Accession Numbers

Sequence data from this article can be found in The Arabidopsis Information Resource data libraries (https://www.arabidopsis.org/index.jsp) with the following accession numbers: *LCD* (AT3G62130), *DCDES* (AT1G48420), *DES1* (AT5G28030), *OASA1* (AT4G14880), *ACT2* (AT3G18780), *ACT7* (AT5G09810), and *ACT8* (AT1G49240).

Supplemental Data

The following supplemental materials are available.

Supplemental Figure S1. Effects of NaHS on Arabidopsis seedling growth.

Supplemental Figure S2. GUS activity and H_2S content assays.

Supplemental Figure S3. Effects of NaHS on the root and root hair growth in *DCDES* gene mutants.

Supplemental Figure S4. Growth phenotypes of OE *LCD-3/oasa1* and OE *LCD-5/oasa1* lines.

Supplemental Figure S5. F-actin cytoskeletal organization assays in leaves of Col-0, OE *LCD-3/oasa1*, and OE *LCD-5/oasa1*.

Supplemental Figure S6. Liquid chromatography-tandem mass spectrometry analysis of the tryptic peptide containing Cys-287 of ACT2 recombinant protein.

Supplemental Figure S7. S-Sulfhydrated rabbit muscle actin protein assays in vivo.

Supplemental Figure S8. Effects of NaHS and NAA on F-actin cytoskeletal organization and actin dynamics.

Supplemental Figure S9. Effects of NaHS and NAA on growth of roots and root hairs.

Supplemental Table S1. Primers used in this study.

Supplemental Movie S1. Time-lapse images of actin filament growth in control conditions.

Supplemental Movie S2. Time-lapse images of actin filament growth in 400 μM NaHS treatment.

Supplemental Movie S3. Time-lapse images of actin filament growth in 600 μM NaHS treatment.

Supplemental Movie S4. Time-lapse images of root hair growth in *act2-1/act2*^{WT} in control conditions.

Supplemental Movie S5. Time-lapse images of root hair growth in *act2-1/act2*^{C287S} in control conditions.

Supplemental Movie S6. Time-lapse images of root hair growth in OE *LCD-5/oasa1* in control conditions.

Supplemental Movie S7. Time-lapse images of root hair growth in OE *LCD-1* in control conditions.

Supplemental Movie S8. Time-lapse images of root hair growth in *act2-1/act2*^{WT} in 500 μM NaHS treatment.

Supplemental Movie S9. Time-lapse images of root hair growth in *act2-1/act2*^{C287S} in 500 μM NaHS treatment.

Supplemental Movie S10. Time-lapse images of root hair growth in OE *LCD-5/oasa1* in 500 μM NaHS treatment.

Supplemental Movie S11. Time-lapse images of root hair growth in OE *LCD-1* in 500 μM NaHS treatment.

Supplemental Materials and Methods S1.

ACKNOWLEDGMENTS

We thank Northwest A&F University, College of Life Sciences' shared instrument platform, and Northwest A&F University Life Science Research Core Services.

Received July 9, 2018; accepted August 21, 2018; published August 30, 2018.

LITERATURE CITED

Alvarez C, Calo L, Romero LC, García I, Gotor C (2010) An O-acetylserine(thiol)lyase homolog with L-cysteine desulfhydrase activity regulates cysteine homeostasis in Arabidopsis. Plant Physiol **152**: 656–669

Álvarez C, Bermúdez MA, Romero LC, Gotor C, García I (2012) Cysteine homeostasis plays an essential role in plant immunity. New Phytol **193**: 165–177

Amann KJ, Pollard TD (2001) Direct real-time observation of actin filament branching mediated by Arp2/3 complex using total internal reflection fluorescence microscopy. Proc Natl Acad Sci USA **98**: 15009–15013

Aroca A, Benito JM, Gotor C, Romero LC (2017a) Persulfidation proteome reveals the regulation of protein function by hydrogen sulfide in diverse biological processes in Arabidopsis. J Exp Bot **68**: 4915–4927

Aroca A, Schneider M, Scheibe R, Gotor C, Romero LC (2017b) Hydrogen sulfide regulates the cytosolic/nuclear partitioning of glyceraldehyde-3-phosphate dehydrogenase by enhancing its nuclear localization. Plant Cell Physiol **58**: 983–992

Aroca Á, Serna A, Gotor C, Romero LC (2015) S-Sulfhydration: a cysteine posttranslational modification in plant systems. Plant Physiol **168**: 334–342

Chen J, Wang WH, Wu FH, You CY, Liu TW, Dong XJ, He JX, Zheng HL (2013) Hydrogen sulfide alleviates aluminum toxicity in barley seedlings. Plant Soil **362**: 301–318

Chen J, Shang YT, Wang WH, Chen XY, He EM, Zheng HL, Shangguan Z (2016) Hydrogen sulfide-mediated polyamines and sugar changes are involved in hydrogen sulfide-induced drought tolerance in *Spinacia oleracea* seedlings. Front Plant Sci **7**: 1173

Christou A, Manganaris GA, Papadopoulos I, Fotopoulos V (2013) Hydrogen sulfide induces systemic tolerance to salinity and non-ionic osmotic stress in strawberry plants through modification of reactive species biosynthesis and transcriptional regulation of multiple defence pathways. J Exp Bot **64**: 1953–1966

Dalle-Donne I, Milzani A, Giustarini D, Di Simplicio P, Colombo R, Rossi R (2000) S-NO-actin: S-nitrosylation kinetics and the effect on isolated vascular smooth muscle. J Muscle Res Cell Motil **21**: 171–181

Dalle-Donne I, Rossi R, Milzani A, Di Simplicio P, Colombo R (2001) The actin cytoskeleton response to oxidants: from small heat shock protein phosphorylation to changes in the redox state of actin itself. Free Radic Biol Med **31**: 1624–1632

Fowler JE, Quatrano RS (1997) Plant cell morphogenesis: plasma membrane interactions with the cytoskeleton and cell wall. Annu Rev Cell Dev Biol **13**: 697–743

Gibbon BC, Kovar DR, Staiger CJ (1999) Latrunculin B has different effects on pollen germination and tube growth. Plant Cell **11**: 2349–2363

Heeg C, Kruse C, Jost R, Gutensohn M, Ruppert T, Wirtz M, Hell R (2008) Analysis of the *Arabidopsis O*-acetylserine(thiol)lyase gene family demonstrates compartment-specific differences in the regulation of cysteine synthesis. Plant Cell **20**: 168–185

Higaki T, Kutsuna N, Sano T, Kondo N, Hasezawa S (2010) Quantification and cluster analysis of actin cytoskeletal structures in plant cells: role of actin bundling in stomatal movement during diurnal cycles in Arabidopsis guard cells. Plant J **61**: 156–165

Hou Z, Wang L, Liu J, Hou L, Liu X (2013) Hydrogen sulfide regulates ethylene-induced stomatal closure in *Arabidopsis thaliana*. J Integr Plant Biol **55**: 277–289

Hussey PJ, Ketelaar T, Deeks MJ (2006) Control of the actin cytoskeleton in plant cell growth. Annu Rev Plant Biol **57**: 109–125

Jia H, Li J, Zhu J, Fan T, Qian D, Zhou Y, Wang J, Ren H, Xiang Y, An L (2013) Arabidopsis CROLIN1, a novel plant actin-binding protein, functions in cross-linking and stabilizing actin filaments. J Biol Chem **288**: 32277–32288

Jia H, Hu Y, Fan T, Li J (2015) Hydrogen sulfide modulates actin-dependent auxin transport via regulating ABPs results in changing of root development in Arabidopsis. Sci Rep **5**: 8251

Jia H, Wang X, Dou Y, Liu D, Si W, Fang H, Zhao C, Chen S, Xi J, Li J (2016) Hydrogen sulfide-cysteine cycle system enhances cadmium tolerance through alleviating cadmium-induced oxidative stress and ion toxicity in Arabidopsis roots. Sci Rep **6**: 39702

Kopriva S (2006) Regulation of sulfate assimilation in Arabidopsis and beyond. Ann Bot **97**: 479–495

Krishnan N, Fu C, Pappin DJ, Tonks NK (2011) H_2S-induced sulfhydration of the phosphatase PTP1B and its role in the endoplasmic reticulum stress response. Sci Signal **4**: ra86

Lam YW, Yuan Y, Isaac J, Babu CV, Meller J, Ho SM (2010) Comprehensive identification and modified-site mapping of S-nitrosylated targets in prostate epithelial cells. PLoS ONE **5**: e9075

Lanza M, Garcia-Ponce B, Castrillo G, Catarecha P, Sauer M, Rodriguez-Serrano M, Páez-García A, Sánchez-Bermejo E, Tc M, Leo del Puerto Y, (2012) Role of actin cytoskeleton in brassinosteroid signaling and in its integration with the auxin response in plants. Dev Cell **22**: 1275–1285

Li J, Jia H, Wang J, Cao Q, Wen Z (2014) Hydrogen sulfide is involved in maintaining ion homeostasis via regulating plasma membrane Na+/H+ antiporter system in the hydrogen peroxide-dependent manner in salt-stress *Arabidopsis thaliana* root. Protoplasma **251**: 899–912

Li ZG, Yang SZ, Long WB, Yang GX, Shen ZZ (2013) Hydrogen sulphide may be a novel downstream signal molecule in nitric oxide-induced heat tolerance of maize (*Zea mays* L.) seedlings. Plant Cell Environ **36**: 1564–1572

Malerba M, Contran N, Tonelli M, Crosti P, Cerana R (2008) Role of nitric oxide in actin depolymerization and programmed cell death induced by fusicoccin in sycamore (*Acer pseudoplatanus*) cultured cells. Physiol Plant **133**: 449–457

McDowell JM, Huang S, McKinney EC, An YQ, Meagher RB (1996) Structure and evolution of the actin gene family in *Arabidopsis thaliana*. Genetics **142**: 587–602

Meagher RB, McKinney EC, Vitale AV (1999) The evolution of new structures: clues from plant cytoskeletal genes. Trends Genet **15**: 278–284

Michelot A, Guérin C, Huang S, Ingouff M, Richard S, Rodiuc N, Staiger CJ, Blanchoin L (2005) The formin homology 1 domain modulates the actin nucleation and bundling activity of *Arabidopsis* FORMIN1. Plant Cell **17**: 2296–2313

Mustafa AK, Gadalla MM, Sen N, Kim S, Mu W, Gazi SK, Barrow RK, Yang G, Wang R, Snyder SH (2009) H_2S signals through protein S-sulfhydration. Sci Signal **2**: ra72

Nick P, Han MJ, An G (2009) Auxin stimulates its own transport by shaping actin filaments. Plant Physiol **151**: 155–167

Papenbrock J, Riemenschneider A, Kamp A, Schulz-Vogt HN, Schmidt A (2007) Characterization of cysteine-degrading and H_2S-releasing enzymes of higher plants: from the field to the test tube and back. Plant Biol (Stuttg) **9**: 582–588

Paul BD, Snyder SH (2012) H_2S signalling through protein sulfhydration and beyond. Nat Rev Mol Cell Biol **13**: 499–507

Qu J, Nakamura T, Cao G, Holland EA, McKercher SR, Lipton SA (2011) S-Nitrosylation activates Cdk5 and contributes to synaptic spine loss induced by beta-amyloid peptide. Proc Natl Acad Sci USA **108**: 14330–14335

Rasmussen I, Pedersen LH, Byg L, Suzuki K, Sumimoto H, Vilhardt F (2010) Effects of F/G-actin ratio and actin turn-over rate on NADPH oxidase activity in microglia. BMC Immunol **11**: 44

Rodríguez-Serrano M, Pazmiño DM, Sparkes I, Rochetti A, Hawes C, Romero-Puertas MC, Sandalio LM (2014) 2,4-Dichlorophenoxyacetic acid promotes S-nitrosylation and oxidation of actin affecting cytoskeleton and peroxisomal dynamics. J Exp Bot **65**: 4783–4793

Romero LC, Aroca MÁ, Laureano-Marín AM, Moreno I, García I, Gotor C (2014) Cysteine and cysteine-related signaling pathways in *Arabidopsis thaliana*. Mol Plant **7**: 264–276

Schafer DA, Jennings PB, Cooper JA (1996) Dynamics of capping protein and actin assembly in vitro: uncapping barbed ends by polyphosphoinositides. J Cell Biol **135**: 169–179

Scheuring D, Löfke C, Krüger F, Kittelmann M, Eisa A, Hughes L, Smith RS, Hawes C, Schumacher K, Kleine-Vehn J (2016) Actin-dependent vacuolar occupancy of the cell determines auxin-induced growth repression. Proc Natl Acad Sci USA **113**: 452–457

Sirko A, Błaszczyk A, Liszewska F (2004) Overproduction of SAT and/or OASTL in transgenic plants: a survey of effects. J Exp Bot **55**: 1881–1888

Staiger CJ (2000) Signaling to the actin cytoskeleton in plants. Annu Rev Plant Physiol Plant Mol Biol **51**: 257–288

Staiger CJ, Gibbon BC, Kovar DR, Zonia LE (1997) Profilin and actin depolymerizing factor: modulators of actin organization in plants. Trends Plant Sci **2**: 275–281

Szumlanski AL, Nielsen E (2009) The Rab GTPase RabA4d regulates pollen tube tip growth in *Arabidopsis thaliana*. Plant Cell **21**: 526–544

Tan BH, Wong PTH, Bian JS (2010) Hydrogen sulfide: a novel signaling molecule in the central nervous system. Neurochem Int **56**: 3–10

von der Ecken J, Müller M, Lehman W, Manstein DJ, Penczek PA, Raunser S (2015) Structure of the F-actin-tropomyosin complex. Nature **519**: 114–117

Wang R (2012) Physiological implications of hydrogen sulfide: a whiff exploration that blossomed. Physiol Rev **92**: 791–896

Yemets AI, Krasylenko YA, Lytvyn DI, Sheremet YA, Blume YB (2011) Nitric oxide signalling via cytoskeleton in plants. Plant Sci **181**: 545–554

Zhou Z, Shi H, Chen B, Zhang R, Huang S, Fu Y (2015) *Arabidopsis* RIC1 severs actin filaments at the apex to regulate pollen tube growth. Plant Cell **27**: 1140–1161

Zhu J, Bailly A, Zwiewka M, Sovero V, Di Donato M, Ge P, Oehri J, Aryal B, Hao P, Linnert M, (2016) TWISTED DWARF1 mediates the action of auxin transport inhibitors on actin cytoskeleton dynamics. Plant Cell **28**: 930–948

Zhu J, Nan Q, Qin T, Qian D, Mao T, Yuan S, Wu X, Niu Y, Bai Q, An L, (2017) Higher-ordered actin structures remodeled by Arabidopsis ACTIN-DEPOLYMERIZING FACTOR5 are important for pollen germination and pollen tube growth. Mol Plant **10**: 1065–1081

Zhu L, Zhang Y, Kang E, Xu Q, Wang M, Rui Y, Liu B, Yuan M, Fu Y (2013) MAP18 regulates the direction of pollen tube growth in *Arabidopsis* by modulating F-actin organization. Plant Cell **25**: 851–867